PB83-188920

Experimental and Theoretical Study of the Wake of a Block-Shaped Vehicle in a Shear-Free Boundary Flow

(U.S.) Environmental Sciences Research Lab.
Research Triangle Park, NC

15 Mar 82

U.S. Department of Commerce
National Technical Information Service
NTIS

TECHNICAL REPORT DATA
(Please read Instructions on the reverse before completing)

1. REPORT NO. EPA-600/J-82-109	2. JOURNAL ARTICLE
3.	PB83-138920
4. TITLE AND SUBTITLE JOURNAL ARTICLE: EXPERIMENTAL AND THEORETICAL STUDY OF THE WAKE OF A BLOCK-SHAPED VEHICLE IN A SHEAR-FREE BOUNDARY FLOW	5. REPORT DATE 1982
	6. PERFORMING ORGANIZATION CODE
7. AUTHOR(S) Robert E. Eskridge and Roger S. Thompson	8. PERFORMING ORGANIZATION REPORT NO. -
9. PERFORMING ORGANIZATION NAME AND ADDRESS Environmental Sciences Research Laboratory, Office of Research and Development, U.S. Environmental Protection Agency, Research Triangle Park, NC 27711	10. PROGRAM ELEMENT NO. ADTA1D/02-1313 (FY-82)
	11. CONTRACT/GRANT NO.
12. SPONSORING AGENCY NAME AND ADDRESS Environmental Sciences Research Laboratory - RTP, NC, Office of Research and Development, U.S. Environmental Protection Agency, Research Triangle Park, NC 27711	13. TYPE OF REPORT AND PERIOD COVERED
	14. SPONSORING AGENCY CODE EPA/600/09

15. SUPPLEMENTARY NOTES

REF: Atmospheric Environment 16(12)2821-2836 (1982)

16. ABSTRACT

The wake of a moving vehicle was simulated using a specially-constructed wind tunnel with a moving floor. A "block-shaped" model vehicle was fixed in position over the test-section floor while the floor moved at the freestream air speed to produce a uniform, shear-free, approach flow. This simulates an automobile traveling along a straight highway under calm atmospheric conditions.

Vertical and lateral profiles of mean and fluctuating velocities and Reynolds stresses in the wake of the vehicle were obtained using a hot-film anemometer with an X-probe. Profiles were taken at distances of 10 to 80 model heights downwind.

A momentum type wake was observed behind the block-shaped vehicle. The wake does not have a simple self-preserving form. However, it is possible to collapse the velocity deficit with one length and one velocity scale.

Two new theories for the velocity deficit are compared to the theory of Eskridge and Hunt (1979). A theory which considered a height-dependent eddy viscosity was found to fit the data best.

Length and velocity scales were found for the longitudinal variation of the turbulent kinetic energy. The lateral variation is described by a two-dimensional numerical fit of the crosswind variation of the data.

17. KEY WORDS AND DOCUMENT ANALYSIS

a. DESCRIPTORS	b. IDENTIFIERS/OPEN ENDED TERMS	c. COSATI Field/Group

18. DISTRIBUTION STATEMENT RELEASE TO PUBLIC	19. SECURITY CLASS *(This Report)* UNCLASSIFIED	21. NO. OF PAGES 17
	20. SECURITY CLASS *(This page)* UNCLASSIFIED	22. PRICE

EPA Form 2220-1 (9-73)

REPRODUCED BY
NATIONAL TECHNICAL
INFORMATION SERVICE
U.S. DEPARTMENT OF COMMERCE
SPRINGFIELD, VA. 22161

EPA-600/J-82-109
JOURNAL ARTICLE

Atmospheric Environment Vol. 16, No. 12, pp. 2821–2836, 1982
Printed in Great Britain

0004-6981/82/122821-16 $03.00/0
Pergamon Press Ltd.

EXPERIMENTAL AND THEORETICAL STUDY OF THE WAKE OF A BLOCK-SHAPED VEHICLE IN A SHEAR-FREE BOUNDARY FLOW

ROBERT E. ESKRIDGE* and ROGER S. THOMPSON

Meteorology and Assessment Division, Environmental Sciences Research Laboratory, U.S. Environmental Protection Agency, Research Triangle Park, NC 27711, U.S.A.

(*First received* 21 *October* 1981 *and received for publication* 15 *March* 1982)

Abstract—The wake of a moving vehicle was simulated using a specially-constructed wind tunnel with a moving floor. A "block-shaped" model vehicle was fixed in position over the test-section floor while the floor moved at the freestream air speed to produce a uniform, shear-free, approach flow. This simulates an automobile traveling along a straight highway under calm atmospheric conditions.

Vertical and lateral profiles of mean and fluctuating velocities and Reynolds stresses in the wake of the vehicle were obtained using a hot-film anemometer with an X-probe. Profiles were taken at distances of 10–80 model heights downwind.

A momentum type wake was observed behind the block-shaped vehicle. The wake does not have a simple self-preserving form. However, it is possible to collapse the velocity deficit with one length and one velocity scale.

Two new theories for the velocity deficit are compared to the theory of Eskridge and Hunt (1979). A theory which considered a height-dependent eddy viscosity was found to fit the data best.

Length and velocity scales were found for the longitudinal variation of the turbulent kinetic energy. The lateral variation is described by a two-dimensional numerical fit of the crosswind variation of the data.

NOMENCLATURE

A	constant, determined from the couple, giving the strength of the wake
a_1, a_2, a_3	constants in turbulent kinetic energy equation
C	couple on the vehicle
C_D	drag coefficient
f	function giving vertical and lateral variation of velocity deficit
F	function describing lateral and vertical variation of turbulent kinetic energy terms in original (EH) theory
F_c	function describing cross-sectional variation of turbulent kinetic energy terms
$\mathbf{F}$	force vector
H	height of the vehicle
$\bar{H}(\zeta)$	normalized function describing vertical variation of eddy viscosity
$H^*(x, z)$	function describing vertical variation of eddy viscosity
$\mathbf{i}$	unit vector in x or x_1 direction
$\mathbf{j}$	unit vector in y or x_2 direction
$\mathbf{k}$	unit vector in z or x_3 direction
$l(x)$	vertical scale length of velocity deficit
$l'(x)$	vertical scale length of turbulence wake
l_E	Eulerian integral length scale
$\mathbf{n}$	outward directed unit normal
p	perturbation pressure
$\mathbf{q}$	three-dimensional velocity vector
s_{ij}	fluctuating rate of strain
S_{ij}	mean rate of strain
u	velocity deficit behind the vehicle defined so that $u \geq 0$
u_{max}	maximum velocity deficit
U	free-stream speed or vehicle speed
$\overline{u'^2}$	x-component of turbulent kinetic energy
$\overline{u'v'}$, $\overline{u'w'}$, etc.	Reynolds stresses
v	y-component of perturbation velocity
$\overline{v'^2}$	y-component of turbulent kinetic energy
W	width of the vehicle
w	z-component of perturbation velocity
$\overline{w'^2}$	z-component of turbulent kinetic energy
(x, y, z), (x_1, x_2, x_3)	right handed coordinates, with x-axis or x_1-axis directed along axis of the wake
$\bar{x}, \bar{y}, \bar{z}$	similarity coordinates used in velocity deficit solution
X_1, X_2, Y_1, Y_2, Z_1	arbitrary points used in control volume analysis
$()_x$	indicates partial derivative with respect to x
α, β	constants relating the decay in the wake to the growth of the length scale
γ	constant in assumed form of eddy viscosity
δ	height of boundary layer in wind tunnel
ζ	similarity coordinate, $z/l(x)$
η	similarity coordinate, $y/l(x)$ or $y/[\lambda WHl(x)]$
λ	constant relating transverse eddy viscosity to the vertical eddy viscosity
Λ_1	constant in original velocity deficit theory
σ	standard deviation of velocity deviations
ν	kinematic viscosity
ν_T	eddy viscosity
ρ	density of dry air
τ_{xy}	shearing stress acting in x direction along a surface normal to the y direction
χ	similarity coordinate, $\chi = y/[W(x/H)^{0.4}]$
$\Psi_{i,j}$	constants in polynomial surface fit
ω	similarity coordinate, $\omega = z/[H(x/H)^{0.4}]$.

1. INTRODUCTION

The dispersion of automobile exhaust near highways is of much current interest. Mathematical models are

* On assignment to EPA from the National Oceanic and Atmospheric Administration.

needed that will accurately predict concentration fields. This study on the structure of the wakes of vehicles was undertaken at the U.S. Environmental Protection Agency's Fluid Modeling Facility to provide information to be used in numerical models of automobile exhaust dispersion. A detailed report of this work is available (Eskridge and Thompson, 1982).

A wind tunnel with a test-section floor that moves at the freestream air speed was constructed to generate a uniform (constant speed with height) approach flow. Scale model vehicles with rotating wheels were held in position in the test section by guys attached to the test-section walls. A vehicle fixed in a uniform flow over a moving floor is aerodynamically equivalent to a vehicle moving down a straight highway through a calm atmosphere.

Automobiles and scale model vehicles have wakes which can be characterized as momentum wakes which contain an organized vortex pair aligned with the axis of the wake. In this paper we are interested in only the momentum wake and, therefore, generally discuss only those data and theories applicable to momentum wakes. The vortex wake of a streamlined car cannot be studied until the pure momentum wakes character is known. To create a "pure" (no mean swirl) momentum wake, block-shaped vehicles of appropriate heights and widths have been used. It should be noted that momentum wakes contain vortices, but in time-averaging the flow the vortices disappear.

A momentum wake's character is determined mainly by the flow field in which it is embedded. Important cases are: flows which are free of limiting walls, and flows which are influenced by a boundary. Free flows may be subdivided further into shear flows and shear-free flows. In addition, wakes in the flows can be subdivided into laminar and turbulent wakes. The classical results for unbounded laminar wakes are given by Goldstein (1938) and a recent theory has been developed by Hunt (1971) for surface-mounted objects. Hunt showed that the strength of the wake for surface-mounted objects is determined by the couple rather than the drag.

Hunt's work was extended by Counihan *et al.* (1974) to describe wakes of two-dimensional objects in a turbulent boundary layer. Castro (1979) has shown that this theory is inapplicable when the wake height approaches that of the boundary layer. However, the wakes of very small two-dimensional objects didn't agree with the theory as well as those behind large two-dimensional blocks. Castro stated that it is unlikely that a constant eddy viscosity model will describe the complex flow in this type of wake.

Theories for wakes behind three-dimensional objects in turbulent boundary layers have been developed by Hunt (1971, 1974), Lemberg (1973) and Hansen and Cermak (1975). Eskridge and Hunt (1979), hereafter referred to as EH, have presented a model of a three-dimensional wake near a moving surface (no shear in the approach flow). Experimental investigations of wakes behind three-dimensional bodies have been carried out recently by Lemberg (1973), Hansen and Cermak (1975), Castro and Robins (1977), Robins and Castro (1977), and Woo *et al.* (1976), among others.

The finding of these studies are summarized in Table 1. This table includes only selected recent results. In wake flows constraints on the exponents of the x-dependence of the velocity deficit and length scale can be derived from the equation of motion and from a control volume analysis, if a self-preserving solution is assumed. Control volume analyses similar to the one in Appendix A can be performed for two-dimensional and three-dimensional objects mounted on a surface or in free flow. If we define a and b as the exponents in: $U_{max}(x) \propto x^{-a}$ and $l(x) \propto x^{b}$, the control volume analyses will show that $a = b$ for wakes of two-dimensional objects in free flow, $a = 2b$ for wakes of three-dimensional objects in free flow and two-dimensional objects on a surface and $a = 3b$ for wakes of three-dimensional objects on a surface. The effects of shear have been ignored for the surface flow. An analysis of the equation of motion, similar to that in Appendix B, using an eddy viscosity that varies as x^{-c}, results in $c = 1 - 2b$. For a constant eddy viscosity, c is equal to zero, and thus $b = 1/2$. In this report, the eddy viscosity was assumed to be proportional to the length scale and the maximum velocity deficit, or $c = a - b$. Most of the entries in Table 1 satisfy these constraints with the only glaring exception being the surface-mounted, three-dimensional object study by Smith *et al.* (1977).

There is an additional complexity in wake flows not yet mentioned. Townsend (1976) hypothesized that a wake flow becomes self-preserving (i.e. one length and one velocity scale will be adequate to describe the velocity, stresses and higher turbulence moments) because the turbulence attains an equilibrium state which depends only on the type of flow and momentum integral, or, in the present case, the couple.

However, Bevilaqua and Lykoudis (1978) have shown that wake strength depends not only on the drag (momentum integral) but also on the structure of the dominant eddies. The flow behind a block-shaped vehicle will shed vortices into the wake like the sphere Bevilaqua and Lykoudis studied. The resulting "memory" effect implies that in a block vehicle wake the turbulent kinetic energy terms ($\overline{u'^2}, \overline{v'^2}, \overline{w'^2}$) will not be self-preserving in the Townsend sense.

2. APPARATUS

2.1. *Wind tunnel*

A wind tunnel was constructed especially for this study. A commercially available conveyor-belt assembly was used for the test-section floor and supporting framework for the entrance, test and exit sections of the wind tunnel. The test section was 4.75 m long (4.15 m of which was moving floor) with a cross section 0.82 m wide and 0.71 m high.

The entrance section had the same cross-section dimensions as the test section. A bellmouth (diameter of 0.22 m) around the perimeter of the entrance directed room air into a section of Vertical™ (Vertical Co., Englewood Co.: paper triangular-cell honeycomb; cell length = 0.15 m and hy-

Table 1. A summary of theoretical and experimental determinations of velocity and turbulence characteristics of wakes behind two- and three-dimensional objects

	Description of the study					Distance dependence			
Investigator or reference	Laminar wake	Turbulent wake	Surface mounted object: fixed floor	Surface mounted object: moving floor	Shear flow	Velocity deficit decay rate	Length scale	Reynolds shear stresses decay rate	$\overline{u'^2}, \overline{v'^2}, \overline{w'^2}$ Decay rate
Two-dimensional objects									
Hunt (1971)	X		X		X	x^{-1}	$x^{1/2}$		
Hunt (1980, pers. comm.)	X			X		x^{-1}	$x^{1/2}$		
Goldstein (1938)	X					$x^{-1/2}$	$x^{1/2}$		
Counihan *et al.* (1974)		X	X		X	x^{-1}		$x^{-3/2}$	$x^{-3/2}$
Castro (1979)		X	X		X	$\sim x^{-1}$		$0(x^{-1})$	$0(x^{-1})$
Schlichting (1960)		X				$x^{-1/2}$	$x^{1/2}$		
Counihan (1971)		X	X			x^{-1}	$x^{0.4}$		
Arya and Shipman (1979)		X	X		X	x^{-1}	$x^{1/2}$	x^{-1}	x^{-1}
Three-dimensional objects									
Smith *et al.* (1977)	X		X		X	$x^{-4/3}$	$x^{1/3}$	$x^{-5/3}$	
Hunt (1974), Woo *et al.* (1977)		X	X		X	$\sim x^{-3/2}$	$x^{3/2}$		
Hunt (1980)	X			X		$x^{-3/2}$	$x^{3/2}$		
Hinze (1975)		X				$x^{-2/3}$	$x^{1/3}$	$x^{-1/3}$	
Eskridge and Hunt (1979)		X		X		$x^{-3/4}$	$x^{3/4}$		$x^{-3/2}$
Lemberg (1973)		X	X		X	$x^{-1.58}$	$x^{1/2}$		$x^{-0.3}$
This study		X		X		$x^{-3/4}$	$x^{3/4}$	$x^{-3/2}$	$x^{-1/2}$

draulic diameter = 0.01 m). Two fiberglas screens (16 × 18 mesh) were placed downwind of the honeycomb to further lower the freestream turbulence.

The moving portion of the test-section floor was the rubber conveyor belt (0.75 m wide). A notched overlapped joint and large end rollers produced a smoothly running belt. Rails along the tops of the walls were installed to support an instrument-traversing mechanism. The longitudinal position of a probe was set manually; vertical and lateral positions were remotely set and read from an operator's desk.

The exit section contained a section of Verticel and a lateral contraction to a 0.71 m wide by 0.71 m high cross section. A cast aluminum fan with three blades (diameter of 0.61 m) was powered by a two-speed (1140/1725 rpm), 250 W electric motor (115 V, 60 Hz). The fan was mounted in a metal "venturi panel" (i.e. shroud) for efficient operation. Baffle plates of different porosities were inserted into a slot just upwind of the fan to fine tune the air speed or to obtain a variety of air speeds for velocity probe calibrations. The maximum air speed, obtained with no baffle plate and the fan motor on high speed, was 4.0 m s^{-1}.

The operating speed of the tunnel during all experiments was 1.9 m s^{-1}; the turbulence intensity (root mean square of the velocity fluctuation divided by the mean speed) was less than 1%.

Homogeneity of the mean flow was checked with the tunnel operating at test condition by measuring vertical profiles at various positions in the test section.

2.2. *Velocity measurements*

Velocities were measured with Thermo-Systems (St. Paul, MN) hot-film anemometers. X-configured probes (model 1243-20) were used to obtain transverse velocity components as well as the streamwise component. The bridge outputs of the anemometers (model 1054-A) were suppressed with signal conditioners (model 1057), attenuated, and sent to the laboratory's Digital Equipment Corporation PDP 11/40 minicomputer. Software in the computer controlled the analog to digital conversion or sampling rate, linearized the signal, and provided real-time displays of results. The probes were calibrated in position on the instrument traversing mechanism against a pitot tube located nearby for determining mean test section velocities obtained with the various baffle plates. The X-probe was oriented to measure either the streamwise and lateral components or the streamwise and vertical components. Calculated values were mean streamwise speed, fluctuating streamwise and transverse components, and the associated Reynolds stress. Most measurements were made at 100 samples s^{-1} for 30 s. A few 10-minute samples at 500 samples s^{-1} were taken at 30 heights downwind of the vehicle at various vertical positions in order to calculate turbulence spectra. From these, an eddy viscosity formulation was derived for use in a theory presented below.

2.3. *Model vehicles*

Simple block-shaped models were constructed of wood; they had proportions of height, width and length of a typical automobile. Each model was mounted on a baseplate with wheels and rubber tires. Approximate scale ratios of 1/32 and 1/8 were used.

The 1/32-scale block-shaped vehicle was patterned on the dimensions of an intermediate size American automobile: height = 0.043 m, width = 0.055 m, length = 0.145 m, ground clearance = 0.009 m and wheel diameter = 0.024 m. The 1/8-scale vehicle was four times as large, in all respects.

2.4. *Wind tunnel blockage effects and Reynolds number independence*

In order to determine if the velocity and turbulence profiles for the large vehicle were affected by blockage in the moving-belt tunnel, several tests were performed with both the small and large vehicles. These experiments were performed in the moving belt tunnel and in two other wind tunnels and it was found that wind tunnel blockage was not a problem and the wake flows are independent of Reynolds number.

3. WAKE THEORY AND MEASUREMENT OF VEHICLE WAKE

3.1. *Review of vehicle wake theory*

A car moving at speed U through a calm atmosphere (windspeed < 1 m s^{-1}) is equivalent to a car held fixed in space over the roadway with the road and air moving past the car at speed U. The coordinate system used here has its origin at the rear of the vehicle. Several heights downwind of the vehicle, beyond the recirculation region, the velocity deviations ($u, v, w \ll U$) from the undisturbed flow are small enough that a perturbation analysis of the equations of motion can be carried out (details are found in EH). The first equation of motion has the following linear form

$$-\rho U\frac{\partial u}{\partial x} = \frac{\partial p}{\partial x} + \frac{\partial \tau_{xz}}{\partial z} + \frac{\partial \tau_{xy}}{\partial y}, \tag{1}$$

where it is assumed that

$$\tau_{xz}/\rho = \nu_T(x)\frac{\partial(U-u)}{\partial z} = -\nu_T(x)\frac{\partial u}{\partial z},$$
$$\tau_{xy}/\rho = -\nu_T(x)\frac{\partial u}{\partial y}, \tag{2}$$

and the eddy viscosity can be estimated as

$$\nu_T(x) \propto l(x)u_{max}(x), \tag{3}$$

where $l(x)$ is a vertical scale length in the wake and $u_{max}(x)$ is the maximum velocity deficit in the wake.

In this (EH) theory it is implicit that the vertical and lateral length scales are identical. The pressure gradient term in (1) can be neglected; the solution to the resulting equation is

$$u = UA\left(\frac{x}{H}\right)^{-3/4}\zeta\exp\left[-(\zeta^2+\eta^2)/8\right], \tag{4}$$

where

$$\zeta = z/l(x),$$
$$\eta = y/l(x), \tag{5}$$
$$l(x) = \gamma AH\left(\frac{x}{H}\right)^{1/4}.$$

γ and A are constants, and H is the height of the vehicle. The value of A can be estimated by approximating the couple acting on the vehicle by the drag on the vehicle times one half the height of the vehicle. This results in (see EH):

$$A \cong \left[\frac{WC_D}{32\pi e^{1/2}H\gamma^3}\right]^{1/4}. \tag{6}$$

The turbulence is estimated by assuming it has a self-preserving form and that the turbulent kinetic energy is proportional to the eddy shear stresses in the wake.

This yields the results:

$$(\overline{u'^2}, \overline{v'^2}, \overline{w'^2}) = (a_1, a_2, a_3)\left(\frac{x}{H}\right)^{-3/2} A^2 F(\zeta, \eta), \quad (7)$$

where $F(\zeta, \eta) = 0.5e^{3/2}[(1-\zeta^2/4)+\zeta^2\eta^2/16]^{1/2}\exp[-(\zeta^2+\eta^2)/8]$

for $(\zeta^2+\eta^2) \geq 12$; $F(\zeta, \eta) = 1$ otherwise. (8)

This theory is reasonable for the velocity field except near the surface, where it is clear that a much stronger shear layer exists than is possible with a constant eddy viscosity. Also, the theory does not allow for obstacles that are wider than they are high. Figure 1 shows a centerline velocity profile taken at $x/H = 60$ compared with the original theory. It is immediately obvious that the wake contains a very strong shear layer near the surface that is incompatible with a constant eddy viscosity in the vertical direction as proposed in (3).

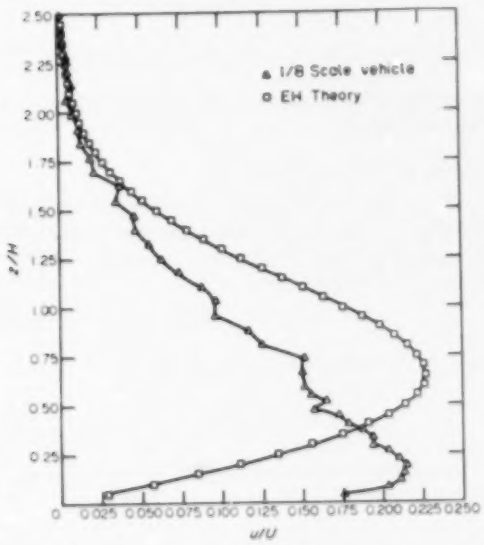

Fig. 1. Vertical profile of velocity deficit at $x/H = 15$, $y = 0$ for 1/8 scale block vehicle and EH theory.

3.2. *Verification of the EH theory*

One of the important predictions of the theory in EH is that the velocity deficit and lateral length scale vary as

$$u \propto \left(\frac{x}{H}\right)^{-3/4} \quad \text{and} \quad l(x) \propto \left(\frac{x}{H}\right)^{1/4}. \quad (9)$$

To determine if the power laws in (9) are satisfied in the wake of the block vehicle, a series of vertical profiles on the centerline at various downwind positions were obtained. The downwind distance, x, was measured from the rear of the vehicle. The velocity deficit was computed for each profile and these are shown in Fig. 2. From these data, the maximum velocity deficit for each distance was determined (Fig. 3). A line corresponding to a $-3/4$ power law is a good fit to the data. A measure of the rate of growth of the length scale of the wake was also determined from the centerline vertical profiles of velocity deficit. According to the original theory and the associated definition of the length scale l, the maximum velocity deficit occurs at a height of $z = 2l$. However, a strong shear near the surface in the velocity deficit profiles made it difficult to use this relationship to determine l. As a measure of the length scale, the height at which the velocity deficit falls to one half the maximum value was determined for each vertical profile. Figure 4 shows that the data do support the 1/4 power relationship. Surprisingly, selection of the rear of the vehicle for the origin proved satisfactory; adjusting the data to a

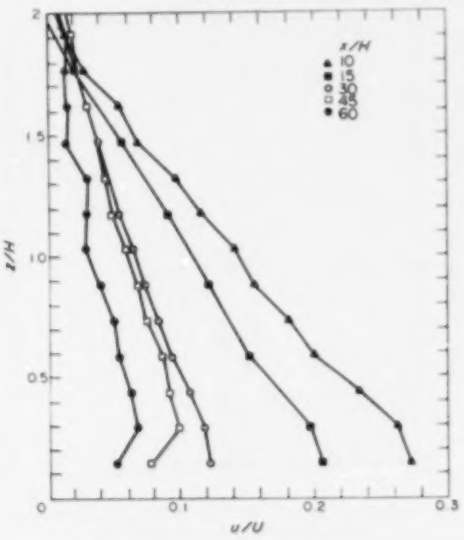

Fig. 2. Vertical profiles of velocity deficit for 1/32 scale vehicle, $y = 0$.

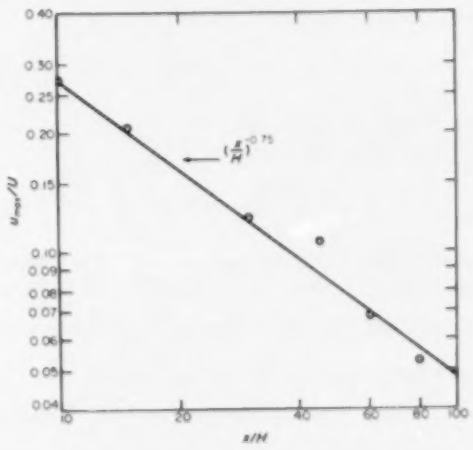

Fig. 3. Decay of maximum velocity deficit with downwind distance.

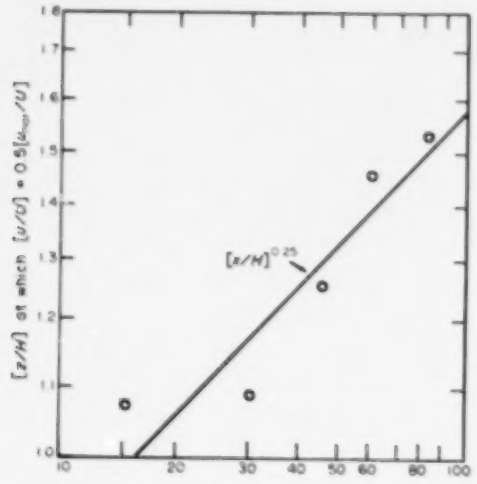

Fig. 4. Rate of growth of the vertical length scale as determined from velocity profiles.

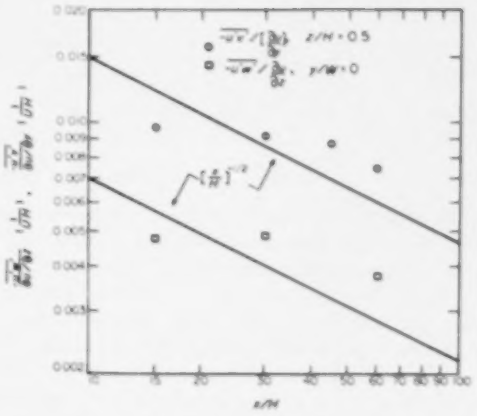

Fig. 5. Measured Reynolds stress divided by velocity shear as a function of downwind distance. Solid lines show theoretical slope, not least squares best fit.

different origin would degrade the curve fits shown in Figs 3 and 4.

The theory in EH assumes an eddy viscosity dependent upon downwind distance or

$$\tau_{xz}/\rho = -\nu_T(x)\frac{\partial u}{\partial z}, \tag{10}$$

where $\nu_T(x) = \gamma l(x) u_{max}(x)$.

Now (10) can be written as

$$\overline{u'w'}\Big/\left(\frac{\partial u}{\partial z}\right) = \gamma l(x) u_{max}(x). \tag{11}$$

The left hand side of (11) was computed from the data on a point by point basis using cubic spline fits to velocity deficit profiles to obtain $\frac{\partial u}{\partial z}$. Near the top of the wake and near the maximum velocity deficit, $\overline{u'w'}$ and $\frac{\partial u}{\partial z}$ become small so that errors in $\overline{u'w'}\Big/\left(\frac{\partial u}{\partial z}\right)$ can be large. However, the ratio was found to be nearly constant over the range between these extremes and an average value was computed for each downwind distance. These are plotted in Fig. 5 which shows that the left hand side of (11) can be reasonably fitted with a line of slope $-1/2$. Since we have already shown that $u_{max} \propto \left(\frac{x}{H}\right)^{-3/4}$, this implies again that

$$l(x) \propto \left(\frac{x}{H}\right)^{1/4}. \tag{12}$$

However, the theory developed in EH does not describe the lateral spread of the wake as well as desired. The EH theory assumes that $l(x)$ is the correct length scale in both the vertical and lateral directions. This is equivalent to assuming the vehicle is as wide as it is high which is incorrect. The line through $\overline{u'v'}\Big/\left(\frac{\partial u}{\partial y}\right)$ in Fig. 5 lies well above the line through $\overline{u'w'}\Big/\left(\frac{\partial u}{\partial z}\right)$ implying different length scales for the vertical and lateral directions.

3.3. *Modified wake theory*

A modified theory which accounts for different scale lengths in the lateral and vertical directions is derived in Appendix B. The solution for the velocity deficit is the same as (4) except that now

$$\eta = yH/\lambda W l(x) \tag{13}$$

and the constant A in (4) is given by

$$A = \left[\frac{C_D}{32\pi e^{1/2}\lambda\gamma^3}\right]^{1/4}, \tag{14}$$

where λ and γ are constants with values of 1.14 and 0.095, respectively. The length scales are

$$l_{vertical} = l(x) \text{ and } l_{lateral} = \lambda\frac{W}{H}l(x). \tag{15}$$

3.4. *Height-dependent-viscosity wake theory*

A further modification to the theory was made in an attempt to improve the agreement between the theory and data for the region of strong shear near the surface. The eddy viscosity was allowed to vary in the z direction as described in Appendix C, where the details of how the height dependence of the eddy viscosity was determined from spectra of $\overline{w'^2}$ are also presented. A numerical solution was then found.

The three theories, original EH, modified lateral length scale, and height-dependent-viscosity, are compared with vertical and lateral velocity deficit profiles in Figs 6 and 7, respectively. The height-dependent eddy viscosity theory lowers the height of the maximum deficit by a factor of nearly two and increases the shear near the surface (Fig. 6). However, the maximum in the data occurs still lower. The improvement in describing the lateral extent of the wake by the

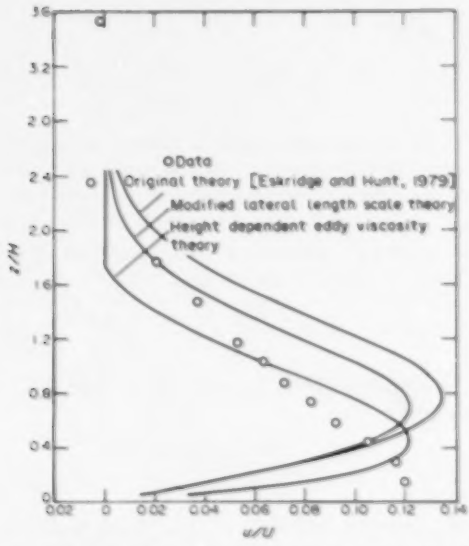

Fig. 6. Theoretical curves and data for vertical profile of velocity deficit for $x/H = 30$ and $y = 0$.

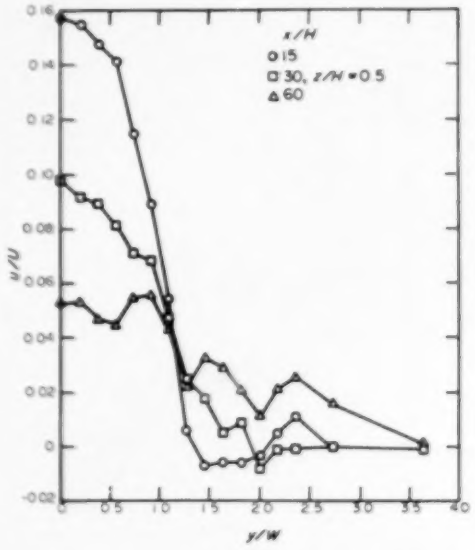

Fig. 8. Lateral profile of velocity deficit at three longitudinal positions at constant ζ.

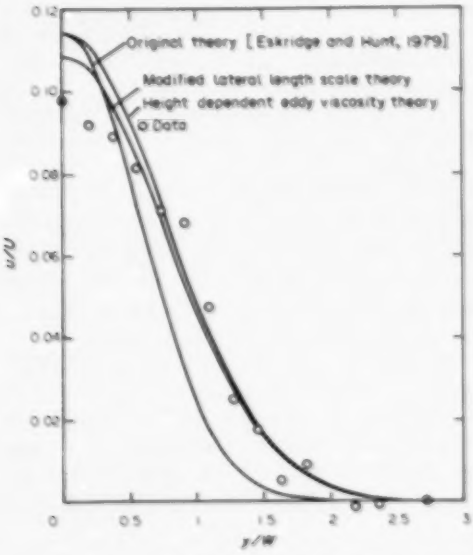

Fig. 7. Theoretical curves and data for lateral profile of velocity deficit for $x/H = 30$ and $z/H = 0.5$.

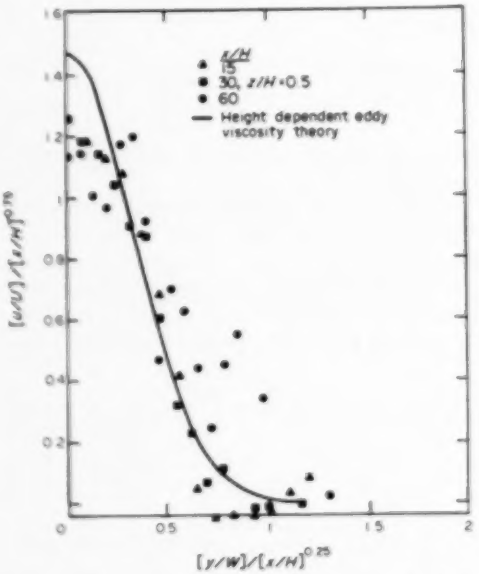

Fig. 9. Theoretical curve and lateral profiles of velocity deficit at constant ζ using similarity coordinates.

modified lateral length scale theory is evident in Fig. 7.

Lateral profiles of velocity deficit at a constant similarity height, ζ, are shown in Fig. 8. These profiles are reduced to similarity coordinates and compared with the height-dependent-viscosity theory in Fig. 9. Vertical profiles of velocity deficit are compared with the height-dependent-viscosity theory in Fig. 10.

2.5. *Turbulent kinetic energy terms*

Preliminary analysis of the fluctuating velocity data indicated that the lateral length scale determined for the velocity deficit would not collapse the profiles of the turbulent kinetic energy components (TKEC). The decay rate of the TKEC was also found to be different than that proposed in EH where complete self-preserving flow was assumed for the wake.

The turbulent energy budget equation can be written (Tennekes and Lumley, 1972)

$$\frac{1}{2}U_j\frac{\partial}{\partial x_j}(\overline{u_iu_i}) = -\frac{\partial}{\partial x_j}\left(\frac{1}{\rho}\overline{u_jp} + \frac{1}{2}\overline{u_iu_iu_j} - 2\nu\overline{u_is_{ij}}\right) - \overline{u_iu_j}S_{ij} - 2\nu\overline{s_{ij}s_{ij}} \quad (16)$$

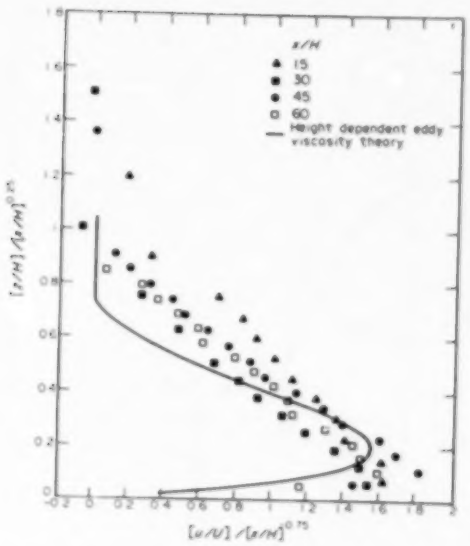

Fig. 10. Theoretical curve and vertical profiles along centerline of velocity deficit using similarity coordinates.

where

$$S_{ij} = \frac{1}{2}\left(\frac{\partial U_i}{\partial x_j} + \frac{\partial U_j}{\partial x_i}\right) \quad \text{and} \quad s_{ij} = \frac{1}{2}\left(\frac{\partial u_i}{\partial x_j} + \frac{\partial u_j}{\partial x_i}\right) \tag{17}$$

and the convention of repeated indices to indicate summation is used.

Assuming as for the velocity deficit solution that longitudinal changes scale with x, while crosswind changes scale with l where $l/x \ll 1$, let $u^2 = 1/3\overline{u_i u_i}$ and make order of magnitude estimates of the terms in (16). Assuming that the turbulence in the wake can be described using one velocity scale and one length scale:

$$U_j \frac{\partial}{\partial x_j}(\tfrac{1}{2}\overline{u_i u_i}) \sim U_\infty u^2/x \qquad \frac{\partial}{\partial x_j}(2\nu\overline{u_i s_{ij}}) \sim u^3/l - (ul/\nu)$$

$$-\frac{\partial}{\partial x_j}\left(\frac{1}{\rho}\overline{u_i p}\right) \sim u^3/l \qquad \overline{u_i u_j} S_{ij} \sim u^3/l$$

$$-\frac{\partial}{\partial x_j}(\tfrac{1}{2}\overline{u_i u_i u_j}) \sim u^3/l \qquad 2\nu\overline{s_{ij} s_{ij}} \sim u^3/l.$$

The order-of-magnitude estimate of the last term, viscous dissipation, is based on experimental evidence for flows with one length scale, as discussed in Tennekes and Lumley. The fourth term is negligible due to the Reynolds number in the denominator, $(ul/\nu) \gg 1$. The estimate for the order of magnitude of the production term $(\overline{u_i u_j S_{ij}})$ is obtained by assuming production is of the same order of magnitude as dissipation. Analysis of the data supported this assumption. Thus, the order of magnitude estimates for all of the terms on the right hand side of (16) are the same, u^3/l. If we say that the combination of the terms on the right side of the same order of magnitude, we can write

$$\frac{Uu^2}{x} \sim \frac{u^3}{l}. \tag{18}$$

If we assume power law forms for the x-dependence of the lateral length scale and decay rate of the TKEC, we can obtain a relation between the exponents. Let the lateral length scale $l \propto x^\alpha$ and $(\overline{u'^2}, \overline{v'^2}, \overline{w'^2}) \propto x^{-\beta}$. Equating the exponents of x for both sides of this relation results in a restriction on α and β.

$$\alpha + \frac{\beta}{2} = 1. \tag{19}$$

A transverse Eulerian integral length scale defined by

$$l_E \equiv \int_0^\infty \frac{\overline{v'(0)v'(y)}}{\overline{v'(0)^2}}\,dy, \tag{20}$$

was computed from data obtained using two x-film probes. This length scale is believed (Tennekes and Lumley, 1972) to be comparable to the Lagrangian integral length scale for most turbulent flows and is thus a measure of the size of the dominant eddies within the wake. Thus, l should be related to l_E; if we empirically determine the x-dependence of l_E and assume $l \propto l_E$ we can evaluate α and β.

The two probes were calibrated and then positioned in the wake of the block vehicle at one half of the vehicle height. One probe was positioned on the wake centerline while the other was moveable in the lateral direction. Profiles of $\overline{v'(0)v'(y)}$ were obtained at downwind distances of $x/H = 15$, 30, 45 and 60. For the greater downwind distances, $\overline{v'^2}$ in the wake was not large compared with background values, so $\overline{v'^2_{\text{background}}}$ was subtracted from $\overline{v'^2(0)}$ for each profile.

The length scale l_E was determined for each of the profiles by a trapezoidal integration. A power-law fit corresponding to $\alpha = 0.40$ is shown in Fig. 11. The value of β computed from (19) is therefore 1.2. Using the computed length scale l_E to minimize the space correlations collapses the data nicely (Fig. 12).

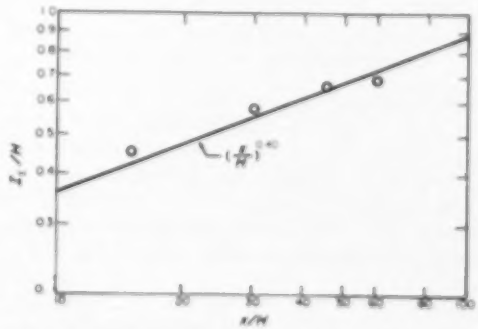

Fig. 11. Length scale determined from fluctuating velocity component, v'.

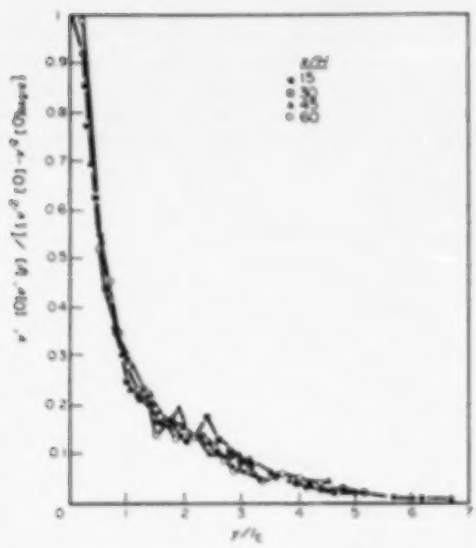

Fig. 12. Correlation of the fluctuating velocity component in similarity coordinates.

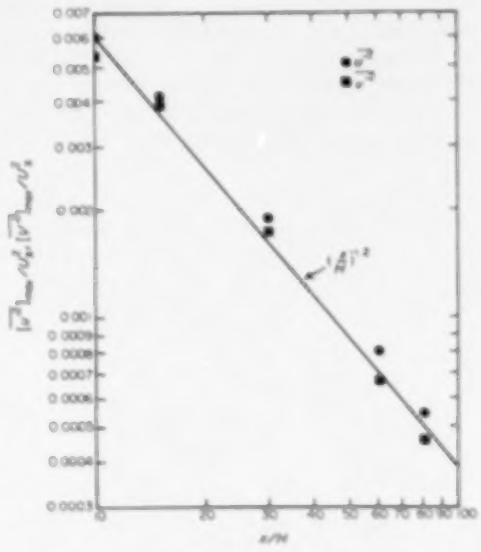

Fig. 13. Longitudinal variation of the maximum values of the turbulent kinetic energy components u'^2 and v'^2 together with least squares linear fit.

The maximum values of $\overline{u'^2}$ and $\overline{v'^2}$ were determined from the vertical centerline profiles obtained at various downwind distances. These are shown in Fig. 13 along with the least squared error fit which gives $\beta = 1.2$, in agreement with the independent estimate from (19).

Thus, the vehicle-generated turbulence in the wake was found to decay as $(x/H)^{-1.2}$ and the lateral length scale was found to grow as $(x/H)^{0.4}$.

The spatial variation of the turbulent kinetic energy is assumed to be given by

$$(\overline{u'^2}, \overline{v'^2}, \overline{w'^2}) = (a_1, a_2, a_3) A^2 U_0^2 \left(\frac{x}{H}\right)^{-1.2} F_e(\chi, \omega), \tag{21}$$

$$A^4 = C_D/(32\pi\epsilon^{1.2}\lambda_T^3), \tag{22}$$

$$\chi = y/[W(x/H)^{0.4}] \quad \text{and} \quad \omega = z/[H(x/H)^{0.4}] \tag{23}$$

and

$$F_e(\chi, \omega)_{\max} = 1.0. \tag{24}$$

At $(x/H) = 30$, detailed measurements were taken in the lateral direction using a 3-min averaging period. The function $F_e(\chi, \omega)$ was determined by a least-squares fit using orthogonal polynomials of the fourth degree (Clark *et al.*, 1963):

$$F_e(\chi, \omega) = \sum_{j=0}^{4} \sum_{i=0}^{2} \chi^{2i} \omega^j \Psi_{2i,j} \tag{25}$$

subject to the following restrictions which result from limiting the domain of F_e to the wake region. $F_e(\chi, \omega) = 0.0$ when:

(i) $|\chi| \geq 0.55$ or $|\omega| \geq 0.64$
(ii) $\chi \leq 0.0$ and $\omega > 1.82\chi + 1.15$
(iii) $\chi > 0.0$ and $\omega > -1.82\chi + 1.15$.

The coefficients in (25) are found in Table 2. From these data the constants in (21) were found to be $a_1 = 0.048$, $a_2 = 0.040$ and $a_3 = 0.030$.

Normalized cross-sections of the turbulence components $\overline{u'^2}$, and $\overline{w'^2}$ were fitted by the orthogonal polynomials of (25) to obtain the contours of F_e (Fig. 14.).

Using (21) with the numerical fit from Table 2, vertical and lateral profiles of the fluctuation velocity

Table 2. Coefficients of polynomial two-dimensional fit to turbulent kinetic energy function F_e

Ψ_{00} =	0.3163277×10^{-1}
Ψ_{01} =	0.1130908×10^{2}
Ψ_{02} =	-0.4320938×10^{2}
Ψ_{03} =	0.6065336×10^{2}
Ψ_{04} =	-0.3218438×10^{2}
Ψ_{20} =	-0.1703226
Ψ_{21} =	-0.8419376×10
Ψ_{22} =	-0.1640925×10^{3}
Ψ_{23} =	0.5061181×10^{3}
Ψ_{24} =	-0.3599435×10^{3}
Ψ_{40} =	0.2386405
Ψ_{41} =	-0.8499160×10^{2}
Ψ_{42} =	0.9322793×10^{3}
Ψ_{43} =	-0.2115435×10^{4}
Ψ_{44} =	0.1360754×10^{4}

components can be estimated. Using similarity coordinates, data at various longitudinal distances can be plotted and compared to these estimates. Figures 15 and 16 show linear and similarity plots of vertical profiles of $\overline{u'^2}$. Figures 17 and 18 show linear and similarity plots of lateral profiles of $\overline{u'^2}$.

3.6. *Shear stresses in the wake*

The wake theories presented in this paper and that of EH make no predictions regarding the decay of the Reynolds shear stresses. From the data for centerline variation of the stresses, it was found that the stresses decay as $(x/H)^{-3/2}$ and hence using the EH value of

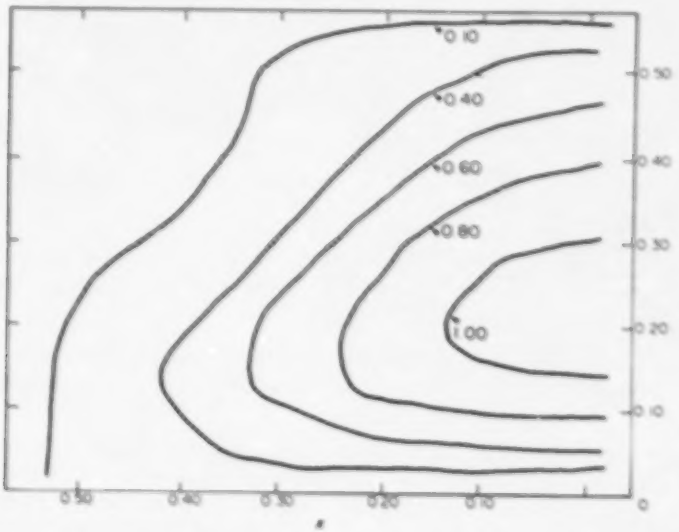

Fig. 14. Cross-section of $F_z(z, o)$ with analyzed isolines of the distribution of F_z.

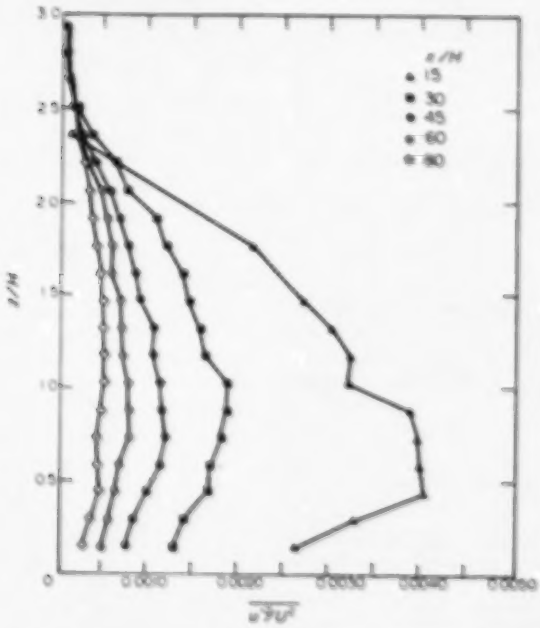

Fig. 15. Measured centerline vertical variation of the turbulent kinetic energy component $\overline{u'^2}$ at various downwind distances.

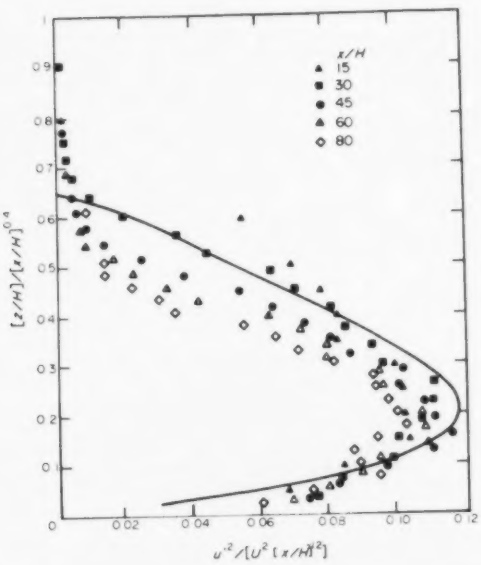

Fig. 16. Measured centerline vertical variation of $\overline{u'^2}$ plotted in TKEC similarity variables compared to Equation 21 (solid line).

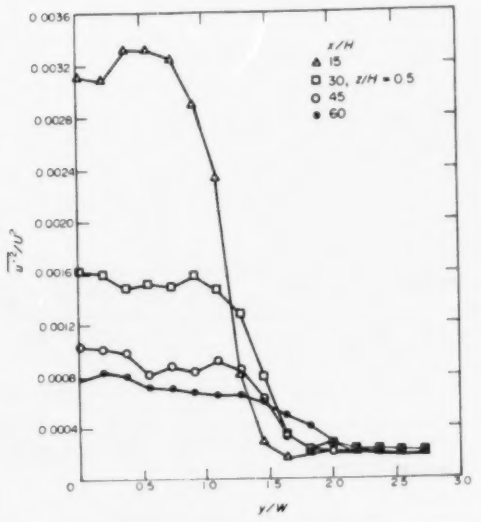

Fig. 17. Measured lateral variation of the turbulent kinetic energy component $\overline{u'^2}$ at various downwind distances.

$(x/H)^{0.25}$ as the length scale growth rate, the data collapse.

4. SUMMARY AND CONCLUSIONS

An experimental study of the wake of a moving vehicle was made using a specially-constructed wind tunnel with a moving floor. A block-shaped model vehicle was fixed in position over the test-section floor while the foor moved at the freestream air speed to produce a uniform, shear-free, approach flow. This

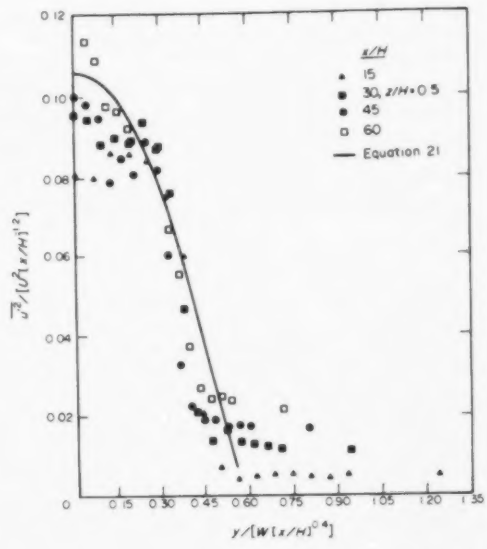

Fig. 18. Measured lateral variation of $\overline{u'^2}$ plotted in TKEC similarity variables compared to Equation 21 (solid line).

simulates an automobile traveling along a straight highway under calm atmospheric conditions.

Vertical and lateral profiles of mean and fluctuating velocities and Reynolds stresses in the wake of the vehicle were obtained using a hot-film anemomenter with an X-probe. Profiles were taken at distances of 10 to 80 model heights downwind of the vehicle.

A momentum wake was observed for the block-shaped vehicle. The wake does not have a simple self-preserving form. However, it is possible to collapse the velocity deficit with one length growth rate and one velocity scale, and the turbulence with different length growth rate and velocity scales.

The velocity deficit behind the vehicle was found to decay as $(x/h)^{-3.4}$ and the length scale to grow as $(x/h)^{1.4}$, confirming the predictions of EH. However, the turbulent kinetic energy components decay as $(x/h)^{-1.2}$ and the turbulent length scale grow as $(x/h)^{0.4}$ instead of the self-preserving solutions of $(x/h)^{-3.2}$ and $(x/h)^{1.4}$ which were predicted.

Velocity deficit solutions are found to the equations of motion for three cases: first, allowing scale-lengths to differ for the lateral and axial directions with constant viscosity (two scale lengths) second, allowing viscosity to vary continuously in the vertical, and finally, a matched solution where viscosity varied linearly near the surface and then was held constant above a given height.

None of the above solutions matched the data in all respects, but the two-scale-length, variable-viscosity solution was the best.

The turbulence decayed longitudinally as $(x/h)^{-1.2}$. To describe the behavior in the lateral and vertical direction a two-dimensional fit of the data was found by least-squares-fit using "orthogonal" polynomials.

Appropriate constants were determined from the data which allow a complete description of the wake turbulence.

Numerical models which predict pollutant concentrations along roadways can be enhanced by including the physical properties of wakes found in this study.

Acknowledgements—The work reported in this paper was influenced by Rex Britter, Ian P. Castro and Julian C. R. Hunt.

REFERENCES

Arya S. P. S. and Shipman M. S. (1979) A model study of boundary layer flow and diffusion over a ridge. *Proc. AMS Fourth Symp. on Turbulence, Diffusion and Air Pollution*, 15–18 Jan., Reno, NV. Am. Meteorological Soc., Boston, MA, pp 584–591.

Bevilaqua P. M. and Lykoudis P. S. (1978) Turbulence memory in self preserving wakes. *J. Fluid Mech.* **89**, 589–606.

Castro I. P. (1979) Relaxing wakes behind surface-mounted obstacles in rough wall boundary layers. *J. Fluid Mech.* **93**, 631–659.

Castro I. P. and Robins A. G. (1977) The flow around a surface-mounted cube in uniform and turbulent streams. *J. Fluid Mech.* **79**, 307–335.

Clark R. E., Kubik R. N. and Phillips L. P. (1963) Orthogonal polynomial least squares surface fit. *Comm. ACM.* **6**, 146–148.

Counihan J., Hunt J. C. R. and Jackson P. S. (1974) Wakes behind two-dimensional surface obstacles in turbulent boundary layers. *J. Fluid Mech.* **64**, 526–563.

Counihan J. (1971) An experimental investigation of the wake behind a two-dimensional block and behind a cube in a simulated boundary layer flow. *C.E.G.B. Lab Note*, RD/LN115/71, Central Electricity Research Laboratories, Leatherhead, England.

Eskridge R. E. and Hunt J. C. R. (1979) Highway modeling. Part I: Prediction of velocity and turbulence fields in the wake of vehicles. *J. appl. Met.* **18**, 387–400.

Eskridge R. E. and Thompson R. S. (1982) Wake of a block vehicle in a shear-free boundary flow—an experimental and theoretical study. Envir. Prot. Agcy. Proj. Rpt., Research Triangle Park, NC.

Goldstein S. (1938) *Modern Developments in Fluid Dynamics*. Oxford University Press, Oxford. (Reprinted by Dover, U.K.)

Hansen A. C. and Cermak J. E. (1975) Vortex-containing wakes of surface obstacles. Project THEMIS Technical report No. 29. (Fluid Dynamics and Diff. Lab. Rpt. No. CER75-76ACH-JEC16,) Colorado State University, Ft. Collins, CO.

Hinze J. O. (1975) *Turbulence*. McGraw-Hill, Maidenhead, U.K.

Hunt J. C. R. (1971) A theory for the laminar wake of a two-dimensional body in a boundary layer. *J. Fluid Mech.* **49**, 159–178.

Hunt J. C. R. (1974) Wakes behind buildings. Aeronautical Research Council (London), Paper ARC35601, Atmos. 229.

Kreyszig E., 1962: *Advanced Engineering Mathematics*. John Wiley, New York, NY.

Lemberg R. (1973) On the wakes behind bluff bodies in a turbulent boundary layer. Ph.D. thesis, University of Western Ontario.

Robins A. G. and Castro I. P. (1977) A wind tunnel investigation of plume dispersion in the vicinity of a surface mounted cube. I. The flow field. *Atmospheric Environment* **11**, 291–297.

Schlichting H. (1960) *Boundary Layer Theory*, Sixth edition, McGraw-Hill, New York, NY.

Smith F. T., Sykes R. I. and Brighton P. W. M. (1977) A two-dimensional boundary layer encountering a three-dimensional hump. *J. Fluid Mech.* **83**, 163–176.

Tennekes H. and Lumley J. L. (1972) *A First Course in Turbulence*, MIT Press, Cambridge, MA.

Townsend A. A. (1976) *The Structure of Turbulent Shear Flow*, second edition, Cambridge University Press, Cambridge, England.

Woo H. G. C., Peterka J. A. and Cermak J. E. (1977) Wind tunnel measurements in the wakes of structures. NASA Contractor Rpt. NASA CR-2806, Colorado State University, Fort Collins, CO.

APPENDIX A: CONTROL VOLUME ANALYSIS

The overturning moment acting on the vehicle can be related to the velocity deficit in the wake with a control volume analysis. Consider the control volume enclosed by the box shown in Fig. A1. The vehicle is excluded from the control volume and the effects of the vehicle on the flow are combined into the overturning moment, C. The small areas where the vehicle tires contact the ground are ignored in the analysis.

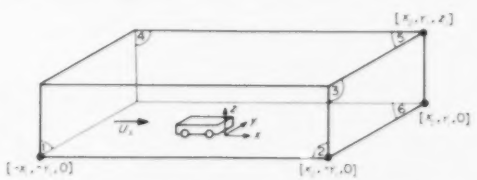

Fig. A1. Control volume for determining the couple.

The vector equation for conservation of moment of momentum is

$$\sum \mathbf{M} = \iint_{c.s.} (\mathbf{r} \times \mathbf{q}) \rho \mathbf{q} \cdot \mathbf{n} \, dA + \frac{\partial}{\partial t} \iiint_{c.v.} \rho (\mathbf{r} \times \mathbf{q}) \, dV \quad \text{(A1)}$$

where $\sum \mathbf{M}$ is the sum of externally acting moments on the control volume, $\mathbf{r}$ is a position vector, $\mathbf{q}$ is the velocity vector $(U - u, v, w)$, $\mathbf{n}$ is an outwardly directed unit vector, $\mathbf{i}, \mathbf{j}, \mathbf{k}$ are the unit vectors in the x, y, z directions respectively, and $\mathbf{M} = \mathbf{r} \times \mathbf{F}$ where $\mathbf{F}$ is a force on the control surface.

Steady state conditions are assumed, i.e. $\frac{\partial}{\partial t}( ) = 0$. Since the overturning moment of the vehicle is about the y-axis, the dot product of $\mathbf{j}$ with (A1) is taken; this, together with an assumption of constant density gives

$$\sum \mathbf{M} \cdot \mathbf{j} = \rho \iint_{c.s.} \mathbf{j} \cdot (\mathbf{r} \times \mathbf{q}) \mathbf{q} \cdot \mathbf{n} \, dA. \quad \text{(A2)}$$

By definition, a shear stress component is positive when the shear stress and vector outwardly normal to the surface of action both act in the positive or negative directions. The shear stress, $\tau_{x_i x_j}$, acts in the x_j direction along a surface normal to the x_i direction.

The external moment about the y-axis resulting from forces acting on Face 1 are due to pressure and shear stress:

$$\begin{aligned}
&\mathbf{j} \cdot (\mathbf{r} \times \mathbf{dF}_{\text{pressure}}) \\
&= \mathbf{j} \cdot [(-\mathbf{i}X_1 + \mathbf{j}y + \mathbf{k}z) \times P(-X_1, y, z)\mathbf{i} \, dy \, dz] \\
&= \mathbf{j} \cdot [-\mathbf{k}y P(-X_1, y, z) \, dy \, dz + \mathbf{j}z P(-X_1, y, z) \, dy \, dz] \\
&= zP(-X_1, y, z) \, dy \, dz
\end{aligned}$$

and

$$\begin{aligned}
&\mathbf{j}\cdot(\mathbf{r}\times\mathbf{dF}_{\substack{\text{shear}\\ \text{stress}}})\\
&=\mathbf{j}\cdot[(-i X_1+\mathbf{j}y+\mathbf{k}z)\times(-j\tau_{xy}(-X_1,y,z)\\
&\quad-\mathbf{k}\tau_{xz}(-X_1,y,z))\,dy\,dz]\\
&=\mathbf{j}\cdot[\mathbf{i}(-y\tau_{xz}(-X_1,y,z)+z\tau_{xy}(-X_1,y,z))\\
&\quad+\mathbf{j}(-X_1\tau_{xz}(-X_1,y,z))+\mathbf{k}(X_1\tau_{xy}(-X_1,y,z))]\,dy\,dz\\
&=-X_1\tau_{xz}(-X_1,y,z)\,dy\,dz.
\end{aligned}$$

Combining and integrating over the area of the face yields the total torque about the y-axis on

Face 1:

$$\int_0^{Z_1}\int_{-Y_1}^{Y_1}[zP(-X_1,y,z)-X_1\tau_{xz}(-X_1,y,z)]\,dy\,dz.$$

In a similar manner the external moments on the other faces are found.

Now the left hand side of (A2) can be written

$$\begin{aligned}
\sum\mathbf{M}\cdot\mathbf{j}=&\int_0^{Z_1}\int_{-Y_1}^{Y_1}\{z[P(-X_1,y,z)-P(X_2,y,z)]\\
&+X_1\tau_{xz}(-X_1,y,z)-X_2\tau_{xz}(X_2,y,z)\}\,dy\,dz\\
&+2\int_{-X_1}^{X_2}\int_0^{Z_1}[z\tau_{yx}(x,Y_1,z)-x\tau_{yz}(x,Y_1,z)]\,dx\,dz^{*}\\
&+\int_{-X_1}^{X_2}\int_{-Y_1}^{Y_1}\{x[P(x,y,Z_1)-P(x,y,0)]\\
&+Z_1\tau_{zx}(x,y,Z_1)\}\,dy\,dx-C,
\end{aligned}\tag{A3}$$

where C is the overturning moment acting on the vehicle which is positive in the y direction; C is the result of all forces from pressure and stress acting on the surfaces of the vehicle.

We also can write the pressure as the sum of a mean and perturbation

$$P(x,y,z)=\overline{P}-p(x,y,z),$$

and we assume the perturbation pressure to be zero far upstream of the vehicle, i.e. $p(X_1,y,z)=0$. The τ's may also be considered perturbation quantities since $\tau_{\text{upstream}}=0$ (uniform flow). Equation (A3) can now be written as

$$\begin{aligned}
\sum\mathbf{M}\cdot\mathbf{j}=&\int_0^{Z_1}\int_{-Y_1}^{Y_1}[zp(X_2,y,z)-X_2\tau_{xz}(X_2,y,z)]\,dy\,dz\\
&+2\int_{-X_1}^{X_2}\int_0^{Z_1}[z\tau_{yx}(x,Y_1,z)\\
&-x\tau_{yz}(x,Y_1,z)]\,dz\,dx\\
&+\int_{-X_1}^{X_2}\int_{-Y_1}^{Y_1}\{x[-p(x,y,Z_1)+p(x,y,0)]\\
&+Z_1\tau_{zx}(x,y,Z_1)\}\,dy\,dx-C.
\end{aligned}\tag{A4}$$

Now the moment of momentum crossing each face of the control surface must be computed, i.e. the right hand side of (A2).

The resulting integrals can be combined to get the right hand side of (A2) noting that due to symmetry, $u(x,Y_1,z)=u(x,-Y_1,z)$, $v(x,Y_1,z)=-v(x,-Y_1,z)$ and $w(x,Y_1,z)=w(x,-Y_1,z)$, the contributions due to surfaces 2 and 4 add. Second order terms like u^2 and uv have been neglected.

Solving (A2) for C and by use of (A3) yields

$$\begin{aligned}
C=&\int_0^{Z_1}\int_{-Y_1}^{Y_1}\{zp(X_2,y,z)\\
&-X_2\tau_{xz}(X_2,y,z)+2z\rho Uu(X_2,y,z)\\
&+X_2\rho Uw(X_2,y,z)\}\,dy\,dz\\
&+\int_{-X_1}^{X_2}\int_{-Y_1}^{Y_1}\{x[-p(x,y,Z_1)+p(x,y,0)]\\
&+Z_1\tau_{zx}(x,y,Z_1)-Z_1\rho Uw(x,y,Z_1)\}\,dy\,dx\\
&+2\int_{-X_1}^{X_2}\int_0^{Z_1}\{[z\tau_{yz}(x,Y_1,z)-x\tau_{yz}(x,X_1,z)]\\
&+zUv(x,Y_1,z)\}\,dz\,dx.
\end{aligned}\tag{A5}$$

Now $|w|\ll|u|$ (from EH), so that $X_2Uw\ll zUu$ in the first integral. Let $Z_1\to\infty$; then $p(x,y,Z_1)\to 0$, $w(x,y,Z_1)\to 0$, and $\tau_{zx}(x,y,Z_1)\to 0$. Also let $Y_1\to\infty$; then $\tau_{yx}(x,Y_1,z)\to 0$ and $v(x,Y_1,z)\to 0$. Let $-X_1\to-\infty$, and since X_2 is arbitrary it can be replaced with x, reducing (A5) to

$$\begin{aligned}
C\simeq&\int_0^{\infty}\int_{-\infty}^{\infty}[zp-\tau_{xz}+2\rho Uuz]\,dy\,dz\\
&+\int_{-\infty}^{\infty}\int_{-\infty}^{\infty}xp(x,y,0)\,dy\,dx.
\end{aligned}\tag{A6}$$

The first equation of motion in perturbation form is

$$-U\frac{\partial u}{\partial x}=\frac{1}{\rho}\frac{\partial p}{\partial x}+\frac{1}{\rho}\frac{\partial\tau_{xz}}{\partial z}+\frac{1}{\rho}\frac{\partial\tau_{xy}}{\partial y}.\tag{A7}$$

Since there are no momentum sources in the control volume from $x=x$ to $x=\infty$, $y=-\infty$ to $y=\infty$, $z=0$ to $z=\infty$, Equation (A7) holds everywhere and can be integrated over this volume. Integrating (A7) with respect to y from $-\infty$ to ∞, integrating with respect to x from x to ∞, multiplying by z and integrating with respect to z from 0 to ∞ yields

$$\begin{aligned}
\int_0^{\infty}\int_{-\infty}^{\infty}zp\,dy\,dz=&-\int_0^{\infty}\int_{-\infty}^{\infty}\rho zuU\,dy\,dz\\
&-\int_0^{\infty}\int_{-\infty}^{\infty}\left[\int_x^{\infty}\tau_{xz}\,dx\right]dy\,dz.
\end{aligned}\tag{A8}$$

And (A6) can now be written as

$$\begin{aligned}
C=&\int_0^{\infty}\int_{-\infty}^{\infty}\left[\rho uUz-x\tau_{xz}-\int_x^{\infty}\tau_{xz}\,dx\right]dy\,dz\\
&+\int_{-\infty}^{\infty}\int_{-\infty}^{\infty}xp(x,y,0)\,dx\,dy\\
=&\int_0^{\infty}\int_{-\infty}^{\infty}\rho uUz\,dy\,dz-\int_{-\infty}^{\infty}x\tau_{xz}\,dz\,dy\\
&-\int_{-\infty}^{\infty}\int_x^{\infty}\int_0^{\infty}\tau_{xz}\,dz\,dx\,dy\\
&+\int_{-\infty}^{\infty}\int_{\infty}^{\infty}xp(x,y,0)\,dx\,dy.
\end{aligned}\tag{A9}$$

Since

$$\int_0^{\infty}\tau_{xz}\,dz=-\nu_T\int_0^{\infty}\frac{\partial u}{\partial z}\,dz=-\nu_T u\Big|_0^{\infty}=0,\tag{A10}$$

(A9) becomes

$$C=\int_0^{\infty}\int_{-\infty}^{\infty}\rho uUz\,dy\,dz+\int_{-\infty}^{\infty}\int_{-\infty}^{\infty}xp(x,y,0)\,dx\,dy.\tag{A11}$$

Now (A7) can be written for distances sufficiently far downwind that the perturbation pressure is negligible (see section 3.1), as

$$U\frac{\partial u}{\partial x}=\nu_T(x)\left[\frac{\partial^2 u}{\partial y^2}+\frac{\partial^2 u}{\partial z^2}\right].\tag{A12}$$

Multiply this by z, integrate the right hand side by parts from

* From symmetry, $\tau_{yx}(x,Y_1,z)=-\tau_{yx}(x,-Y_1,z)$, etc.

$z = 0$ to ∞ and then integrating with respect to y from $-\infty$ to ∞, to get

$$\frac{\partial}{\partial x}\int_{-\infty}^{\infty}\int_{0}^{\infty}\rho u U z\,dy\,dz = 0$$

or

$$\int_{-\infty}^{\infty}\int_{0}^{\infty}\rho u U z\,dy\,dz = \text{constant, at large } x. \quad \text{(A13)}$$

The couple on the vehicle for a given situation is a value that could be determined by measurement. At distances sufficiently downwind for (A13) to hold, we can therefore conclude that the second integral on the right hand side of (A12) is a constant, not a function of x. It is assumed that the second integral in (A11) is small and therefore the couple on the vehicle determines the wake strength. Hunt (1974) indicates that the second integral can be neglected for three-dimensional objects.

When the stress is approximated by a viscosity that varies in the vertical direction the analysis is similar to that given with the following modifications. Equation (1) in section 3.1 takes the form

$$\rho U\frac{\partial u}{\partial x} = \nu_T(x)\left[\frac{\partial}{\partial z}\left(H^*(x,z)\frac{\partial u}{\partial z}\right)+\frac{\partial^2 u}{\partial y^2}\right], \quad \text{(A14)}$$

where $H^*(x,z)$ is the vertical dependence of viscosity. Multiplying by z and integrating with respect to y and z yields

$$\frac{\partial}{\partial x}\int_{-\infty}^{\infty}\int_{0}^{\infty} z\rho U u\,dz\,dy = \nu_T(x)\int_{-\infty}^{\infty}\left[-\int_{0}^{\infty}H^*(x,z)\frac{\partial u}{\partial z}dz\right]dy. \quad \text{(A15)}$$

(A15) then gives an integral constraint on the definition of $H^*(x,z)$, i.e. we must choose $H^*(x,z)$ to satisfy

$$\int_{0}^{\infty}H^*(x,z)\frac{\partial u}{\partial z}dz = 0 \quad \text{(A16)}$$

in order for (A13) to be valid. The analysis of the couple would be the same since (A10) would take the form

$$\int_{0}^{\infty}\tau_{xz}dz = -\nu_T(x)\int_{0}^{\infty}H^*(x,z)\frac{\partial u}{\partial z}dz = 0. \quad \text{(A17)}$$

APPENDIX B: MULTI-SCALE WAKE THEORY

The following derivation follows very closely the form in EH. The assumptions are the same as those given in Section 3.1 and we use the same notation.

The linearized first equation of motion is given

$$-\rho U\frac{\partial u}{\partial x} = \frac{\partial p}{\partial x}+\frac{\partial \tau_{xz}}{\partial z}+\frac{\partial \tau_{xy}}{\partial y}, \quad \text{(B1)}$$

where the shearing stresses are assumed to have the form

$$\tau_{xz}/\rho = -\nu_T\frac{\partial u}{\partial z} \quad \text{and} \quad \tau_{xy}/\rho = -\lambda^2\frac{W^2}{H^2}\nu_T\frac{\partial u}{\partial y}, \quad \text{(B2)}$$

where W and H are the width and height of the vehicle, respectively, and

$$\nu_T(x) = \gamma l(x)u_{max}(x). \quad \text{(B3)}$$

We have allowed for different length scales in the lateral and vertical and assume them to be related by

$$l_{vertical} = l(x) \quad \text{and} \quad l_{lateral} = \lambda\frac{W}{H}l(x). \quad \text{(B4)}$$

As in EH it can be shown that $\partial p/\partial x$ can be neglected. (B1) now becomes

$$U\frac{\partial u}{\partial x} = \nu_T(x)\left[\frac{\partial^2 u}{\partial z^2}+\lambda^2\frac{W^2}{H^2}\frac{\partial^2 u}{\partial y^2}\right]. \quad \text{(B5)}$$

Assume a solution of the form

$$u = U\left(\frac{x}{H}\right)^{-m}Af(z/l(x),\ yH/\lambda Wl(x)), \quad \text{(B6)}$$

where A is a constant to be determined and $f \leqslant 1$. Now, let

$$\zeta = z/l(x) \quad \text{and} \quad \eta = yH/\lambda Wl(x) \quad \text{(B7)}$$

and substitute (B6) into (B5) to get

$$U\left(\frac{-m}{H}\right)\left(\frac{x}{H}\right)^{-1}f(\zeta,\eta) - U\frac{1}{l(x)}\frac{dl(x)}{dx}[\zeta f_\zeta+\eta f_\eta]$$
$$= \frac{\nu_T(x)}{l^2(x)}[f_{\zeta\zeta}+f_{\eta\eta}]. \quad \text{(B8)}$$

Along a path where $f = f_{max} = 1$, one finds

$$f_\zeta = f_\eta = 0 \quad \text{and} \quad f_{\zeta\zeta} = \text{constant}, f_{\eta\eta} = \text{constant}. \quad \text{(B9)}$$

Hence

$$U\left(\frac{-m}{H}\right)\left(\frac{x}{H}\right)^{-1} = \frac{\nu_T(x)}{l^2(x)} \times \text{constant} \quad \text{(B10)}$$

which implies

$$\frac{U}{x} \propto \frac{\nu_T(x)}{l^2(x)} \quad \text{or} \quad l(x) \propto x u_{max}(x). \quad \text{(B11)}$$

From the control volume analysis given in Appendix A the overturning couple on the vehicle is given by

$$C = \rho\int_{-\infty}^{\infty}\int_{0}^{\infty} zuU\,dz\,dy \cong \frac{\rho C_D}{4}U^2H^2W. \quad \text{(B12)}$$

The approximation on the right is obtained by taking the overturning moment to be the drag force times one-half the vehicle height.

If we substitute (B6) into (B12), the integral constraint becomes

$$C = \lambda\frac{W}{H}U^2A\left(\frac{x}{H}\right)^{-m}l^3(x)\int_{-\infty}^{\infty}\int_{0}^{\infty}\zeta f(\zeta,\eta)d\zeta\,d\eta. \quad \text{(B13)}$$

Hence,

$$C \propto \lambda\frac{W}{H}U^2A\left(\frac{x}{H}\right)^{-m}l^3(x) \quad \text{or} \quad l^3(x)\left(\frac{x}{H}\right)^{-m} = \text{constant}. \quad \text{(B14)}$$

From (B11) and (B14)

$$x^3x^{-3m}x^{-m} = \text{constant}, \quad \text{(B15)}$$

which implies that $m = 3/4$. Thus, we have $u_{max}(x) \propto x^{-3/4}$ and $l(x) \propto x^{1/4}$. If we define $l(x) = \gamma AH(x/H)^{1/4}$, and note that $u_{max} = AU(x/H)^{-3/4}$, (B8) becomes

$$f_{\zeta\zeta}+f_{\eta\eta}+\frac{1}{4}(\zeta f_\zeta+\eta f_\eta)+\frac{3}{4}f = 0 \quad \text{(B16)}$$

describing the behavior of the velocity deficit in all planes normal to the wake.

The solution to (B16) is known (EH) to be

$$f(\zeta,\eta) = \frac{\Lambda_1}{(8\pi)^{1/2}}\zeta\exp[-(\zeta^2+\eta^2)/8], \quad \text{(B17)}$$

where $\Lambda_1 = (2\pi e)^{1/2}$.

The constant A can now be computed using (B12) and (B17):

$$\frac{C_D}{4}U^2H^2W = Uu_{max}\left(\frac{\lambda W}{H}\right)\Lambda^3\int_{-\infty}^{\infty}\int_{0}^{\infty}\zeta f(\zeta,\eta)d\zeta\,d\eta, \quad \text{(B18)}$$

yielding

$$A = \left[\frac{C_D}{32\pi e^{1/2}\lambda\gamma^3}\right]^{1/4}. \quad \text{(B19)}$$

The solution for the velocity deficit is now known (B6, B17 and B19) except for two constants γ and λ.

To determine λ we use (B2):

$$v_T(x) = \overline{u'w'}\Big/\left(\frac{\partial u}{\partial z}\right) \tag{B20}$$

and

$$\lambda^2 \frac{W^2}{H^2} v_T(x) = \overline{u'v'}\Big/\left(\frac{\partial u}{\partial y}\right). \tag{B21}$$

The right hand sides of (B20) and (B21) have been determined at various downwind distances by fitting vertical and lateral velocity profiles with cubic splines which were differentiated to determine the velocity gradients. Above the maximum velocity deficit the velocity gradient was well behaved and averaged values of $-\overline{u'w'}/(\partial u/\partial z)$ and $-\overline{u'v'}/(\partial v/\partial z)$ are plotted in Fig. 5. The straight lines fitting these points are least squares linear fits to the data.

The value of λ can now be determined by using, say, $x/H = 10$ and the fitted values to the profiles giving $\lambda = 1.14$. To determine γ we use (B3) and (B19) and that at $x/H = 10$, $v_T^2/U^2H^2 = (0.007)^2$. This results in $\gamma = 0.095$.

APPENDIX C: HEIGHT-DEPENDENT-VISCOSITY WAKE THEORY

Assume the perturbation equation of motion (B1) can be written as

$$U\frac{\partial u}{\partial x} = \frac{\partial}{\partial z}\left(H^*(x,z)v_T(x)\frac{\partial u}{\partial z}\right) + \frac{\partial}{\partial y}\left(\lambda^2\frac{W^2}{H^2}v_T(x)\frac{\partial u}{\partial y}\right), \tag{C1}$$

where $H^*(x, z)$ is some function of height having a continuous derivative. From Appendix B we can express (C1) and its solution as

$$\frac{\partial u}{\partial x} = \bar{x}^{-1.2}\left[\frac{\partial}{\partial z}\left(H^*(x,z)\frac{\partial u}{\partial z}\right) + \frac{\partial^2 u}{\partial y^2}\right] \tag{C2}$$

and

$$u = UA\left(\frac{x}{H}\right)^{-3.4} f(\bar{z}/l(x), \bar{y}/l(x)) \tag{C3}$$

where

$$\bar{x} = (x/H),\ \bar{z} = z/\gamma AH \quad \text{and} \quad \bar{y} = y/\lambda\gamma AW. \tag{C4}$$

Substituting (C3) into (C2) yields for f the partial differential equation ($\tilde{H}(\zeta)$ is the transform of $H^*(x, z)$ and $\tilde{H}(\zeta) \leqslant 1$)

$$\tilde{H}(\zeta)f_{\zeta\zeta} + f_{\eta\eta} + \tilde{H}_\zeta(\zeta)f_\zeta + \frac{1}{4}(\zeta f_\zeta + \eta f_\eta) + \frac{3}{4}f = 0. \tag{C5}$$

Equation (C5) can be solved in part by assuming it is separable, i.e.

$$f(\zeta, \eta) = T(\zeta)Y(\eta). \tag{C6}$$

This yields

$$Y(\eta) = C_1 e^{-\eta^2/8}$$

and

$$\tilde{H}T'' + \frac{3}{4}T' + \tilde{H}'T' + \frac{T}{2} = 0, \tag{C7}$$

where (C7) is subject to the boundary conditions

$$T(0) = 0,\ T_{\max}(\zeta) = 1. \tag{C8}$$

Analytic solutions are easily found for (C7) and (C8) only when $\tilde{H}(\zeta)$ is a simple function. Hence, (C7) and (C8) have been solved numerically using the Runge–Kutta–Nystrom method (Kreyszig, 1962).

To arrive at an expression for $\tilde{H}(\zeta)$ we have taken data along the centerline ($y = 0$) at $x/H = 30$ for $z/H = 0.15, 0.29, 0.44, 0.59, 0.74, 0.88, 1.03, 1.18, 1.32, 1.47, 1.76, 2.06, 2.35$ and 2.94, which allowed us to compute spectra at each height. We further assumed that

$$v_T \propto (\overline{w'^2})^{1/2}U/N \quad \text{or} \quad \tilde{H}(\zeta) \propto (\overline{w'^2})^{1/2}U(\zeta)/N, \tag{C9}$$

where $(\overline{w'^2})^{1/2}$ is the standard deviation of the vertical velocity, $U(\zeta)$ is the mean wind speed at height ζ and N is the frequency containing the maximum energy. A best N was determined for each height from the spectra together with estimated upper and lower bounds. The product $(\overline{w'^2})^{1/2}U(\zeta)N$ is normalized by dividing by its maximum value. These results together with error ranges are plotted in Fig. C1. The following function describing $\tilde{H}(\zeta)$ was found by

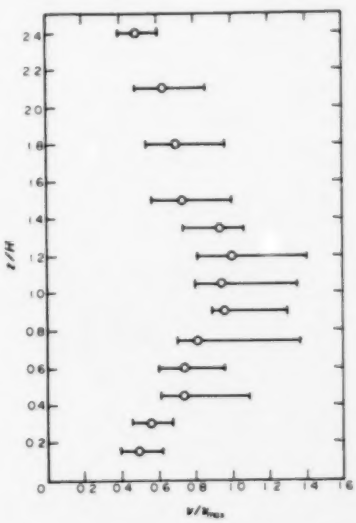

Fig. C1. Vertical variation of the eddy viscosity determined from the spectral data.

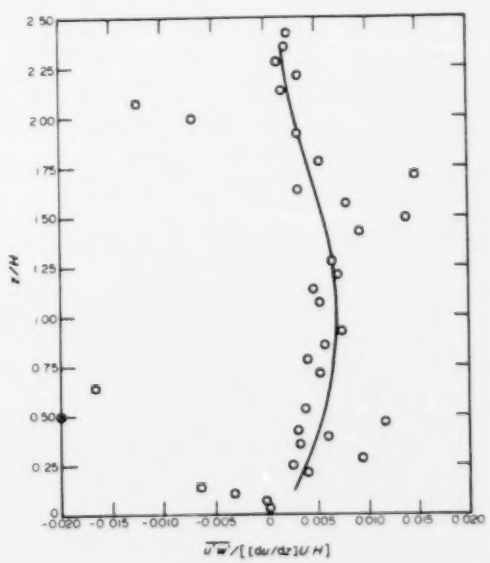

Fig. C2. Vertical variation of the eddy viscosity determined from the Reynolds stress $\overline{u'w'}$.

a least-squares fit to the data in Fig. C1, after changing variables from z/H to ζ.

$$\tilde{H}(\zeta) = 0.2616 + 0.4874\zeta - 0.09617\zeta^2 + 0.006193\zeta^3 - 0.0001305\zeta^4. \quad \text{(C10)}$$

In order to describe the vertical change in viscosity we plotted $\overline{u'w'}/(\partial\bar{u}/\partial z)$ from data taken with the 1/8 scale block vehicle. The vertical velocity gradient was estimated at each point with a cubic spline fit. The estimate naturally contains error and is partly responsible for the scatter in Fig. C2. Careful study of Figs C1 and C2 shows that, except for scatter, the trends in both plots are the same and the maximum occurs near $z/H = 1.25$ in both plots.